the 3′ side in both LCL and SF (Fig. 3B). Although such a chimeric clone would have been produced by a splice error, this indicated that duplicated exon 1.4 at the distal nonphysiological position functioned as a transcription start site.

Characterization of the cryptic deletions

In cases from family C, long PCR products were obtained with the P7 primer and the P9 primer, and the deletion junction was determined by direct sequencing with the P8 primer (Fig. 3C). The deleted region was 211,631-bp long and involved exons 2–43 of *DMXL2* and exons 5–10 of *GLDN*. The two breakpoints resided within a LINE 1 repeat sequence and a nonrepeat sequence respectively, and a 33-bp segment with a LINE 1 repeat sequence was inserted to the fusion point. In cases from families D–F, long PCR products were obtained by sequential amplifications with the P12 primer and the P14 primer and with the P13 primer and the P14 primer, and an identical deletion was identified by direct sequencing with the P13 primer (Fig. 3D). The deletion was 165,901-bp long and involved exons 2–43 of *DMXL2*. The fusion occurred between two LINE 1 repeat sequences with an overlap of a 12-bp segment.

Sequence analysis of the 5′-RACE products obtained from LCL of cases 5 and 6 (family C) and from SF of case 9 (family D) and case 10 (family E) revealed the presence of a few clones with *DMXL2* exon 1 (2–5%), together with multiple clones with a single wild-type *CYP19A1* exon 1 (Fig. 3, C and D). Such a chimeric mRNA clone was absent from control materials. Furthermore, *DMXL2* exon 1 was found to be accompanied by a promoter-compatible sequence (Supplemental Fig. 2). This indicated a cryptic usage of *DMLX2* exon 1 as an alternative *CYP19A1* transcription start site in cases with deletions. Notably, because of the presence of the translation start codon on *DMXL2* exon 1, mRNAs of the *DMLX2/CYP19A1* chimeric genes are predicted to produce two proteins, *i.e.* CYP19A1 protein and an apparently nonfunctional 47-amino acid protein with a termination codon on *CYP19A1* exon 2, when the translation started from the initiation codons on *CYP19A1* exon 2 and on *DMLX2* exon 1, respectively. Furthermore, mRNA destined to yield the 47-amino acid protein is predicted to undergo nonsense-mediated mRNA decay (NMD) because it satisfies the condition for the occurrence of NMD (12).

Relative mRNA levels of *CYP19A1* and its neighboring genes

CYP19A1 showed a markedly high expression in the placenta and a relatively weak expression in a limited number of tissues including hypothalamus and ovary. By contrast, *DMXL2* was expressed in a range of tissues with some degree of variation as well as *CGNL1*, *MAPK6*, *TMOD3*, and *TLN2* (Fig. 4).

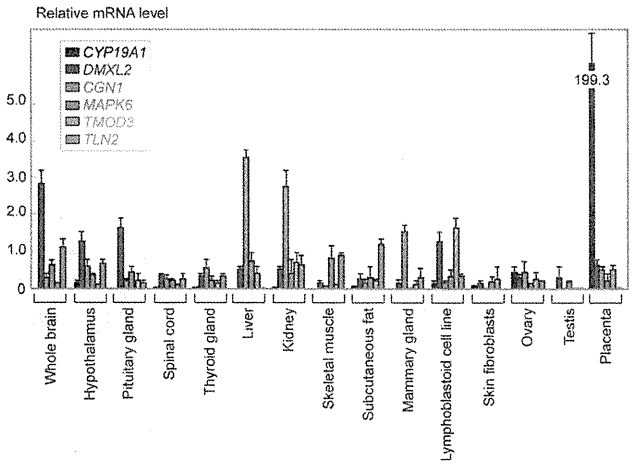

FIG. 4. Expression patterns of *CYP19A1* and the five neighboring genes involved in the chimeric gene formation. Relative mRNA levels against *TBP* are shown.

Discussion

We identified cryptic duplications of the *CYP19A1* promoter region and deletions of the *CYP19A1* upstream region in cases with AEXS. The tandem duplications would have caused *CYP19A1* overexpression because of an increased number of the wild-type transcription start sites. Indeed, because a rare mRNA variant with exon I.4 and exon I.8 was identified, this implies that duplicated exons 1 at the distal nonphysiological position can also function as transcription start sites. Similarly, the deletions would have caused *CYP19A1* overexpression because of a cryptic usage of *DMXL2* exon 1 with a putative promoter function as an extra transcription start site for *CYP19A1*. Indeed, because a few clones with *DMXL2* exon 1 and *CYP19A1* exon 2 were identified, this confirms the formation of a *DMXL2/CYP19A1* chimeric gene. Thus, our results suggest for the first time that duplications of a physiological promoter and deletions of an upstream region can cause overexpression of a corresponding gene and resultant human genetic disease.

Such cryptic genomic rearrangements can be generated by several mechanisms. The tandem duplication in families A and B would be formed by a replication-based mechanism of fork stalling and template switching that occurs in the absence of repeat sequences and is associated with microhomology (13). The deletion in family C is explained by nonhomologous end joining that takes place between nonhomologous sequences and is frequently accompanied by an insertion of a short segment at the fusion point (13).

The deletion in families D–F is compatible with a repeat sequence mediated nonallelic intrachromosomal or interchromosomal recombination (13). Thus, in conjunction with the previously identified four cryptic inversions that are also explainable by fork stalling and template switching or nonallelic recombination (8), genomic sequence around *CYP19A1* appears to harbor particular motifs that are vulnerable to replication and recombination errors.

To date, three types of cryptic genomic rearrangements have been identified in patients with AEXS, *i.e.* duplication type, deletion type (two subtypes), and inversion type (four subtypes) (Fig. 5). Here, although the deletion and the inversion types are associated with heterozygous impairment of neighboring genes (deletion or disconnection between noncoding exon(s) and coding exons), the phenotypes of patients are well explained by excessive *CYP19A1* activity alone. Thus, haploinsufficiency of these neighboring genes would not have a major clinical effect.

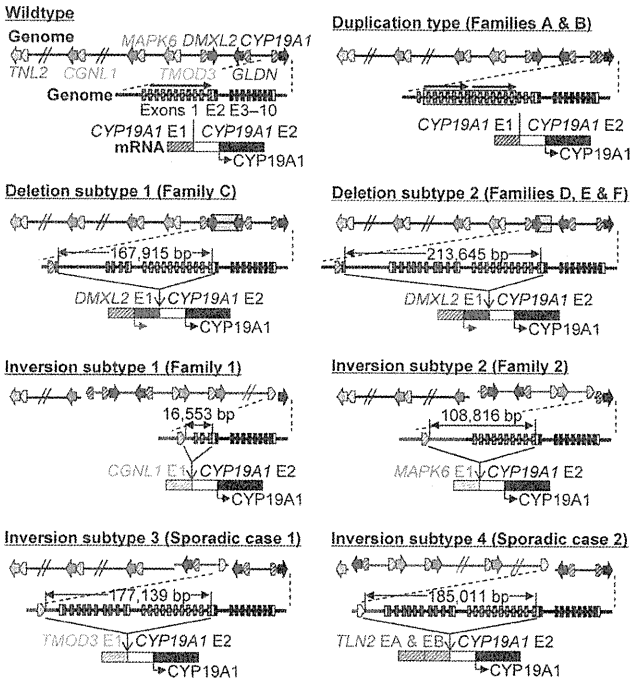

FIG. 5. Schematic representation of the rearranged genome and mRNA structures. The *white* and *black boxes* of *CYP19A1* exon 2 show untranslated region and coding region, respectively (for details, see Supplemental Fig. 1). For the duplication type and the deletion subtypes, see Fig. 3, C and D, for details. For genome, the *striped* and *painted arrows* indicate noncoding and coding exons, respectively (5′→3′). The inverted genomic regions are delineated in *blue lines*. For mRNA, *colored striped boxes* represent noncoding regions of each gene. For *TLN2*, exons A and B correspond to the previously reported exons 1 and 2 (8); because current exon 1 in the public database indicates the first coding exon, we have coined the terms exons A and B for the noncoding exons. The deletion and inversion types are associated with heterozygous impairment of neighboring genes [deletion or disconnection between noncoding exon(s) and the following coding exons]. The inversion subtype 1 is accompanied by inversion of eight of the 11 *CYP19A1* exons 1, and the inversion subtype 2 is associated with inversion of the placenta-specific *CYP19A1* exon I.1.

For the deletion and inversion types, two factors should be considered. One factor is expression patterns of each chimeric gene. In this regard, the five genes involved in the formation of chimeric genes are widely expressed, with some degree of variation (Fig. 4). Furthermore, *in silico* analysis revealed promoter-compatible sequences around exon 1 of *DMXL2*, *CGN1*, *MAPK6*, and *TMOD3* in multiple cell types, although such sequences remain to be identified for noncoding exons of *TLN2* (Supplemental Fig. 2). These findings imply that the chimeric genes show wide expression patterns because expression patterns of chimeric genes would follow those of the original genes.

The other factor is expression dosage of each chimeric gene. In this context, the *DMXL2/CYP19A1* chimeric mRNA was identified only in 2–5% of transcripts from SF, whereas the *CGNL1/CYP19A1* chimeric mRNA and the *TMOD3/CYP19A1* chimeric mRNA accounted for 89–100% and 80% of transcripts from SF, respectively (no data for the *MAPK6/CYP19A1* and the *TLN2/CYP19A1* chimeric genes) (5). This difference is obviously inexplicable by the relative expression level in SF that is grossly similar between *DMXL2* and *TMOD3* and is quite low for *CGNL1* (Fig. 4). In this regard, it is notable that a translation start codon and a following coding region are present on exon 1 of *DMXL2* (Fig. 5). It is likely that *DMXL2/CYP19A1* chimeric mRNA transcribed by the *DMXL2* promoter preferentially recognized the natural start codon on *DMXL2* exon 1 and underwent NMD and that rather exceptional chimeric mRNAs, which recognized the start codon on *CYP19A1* exon 2, were identified by 5′-RACE. By contrast, such a phenomenon would not be postulated for the inversion-mediated chimeric mRNA because of the absence of a translation start codon on the fused exon 1 of *CGNL1* and *TMOD3* (as well as exon 1 of *MAPK6* and exons A and B of *TLN2*) (Fig. 5). For the *CGNL1/CYP19A1* chimeric gene, furthermore, the physical distance between *CGNL1* exon 1 and *CYP19A1* exon 2 is short, and whereas a splice competition may be possible between exon 1 of neighboring genes and original *CYP19A1* exons 1, eight of 11 *CYP19A1* exons 1 including exon I.4 functioning as the major promoter in SF have been disconnected from *CYP19A1*-coding exons by inversion. These structural characters would have also contributed to the efficient splicing between *CGNL1* exon 1 and *CYP19A1* exon 2 (14). In this context, although the *CGNL1/CYP19A1* chimeric gene is associated with functional loss of eight *CYP19A1* exons 1 and the resultant reduction of *CYP19A1* expression in *CYP19A1*-expressing tissues, overall aromatase activity would be increased

by the wide expression of the chimeric gene. These structural properties would primarily explain the difference in the expression dosage of chimeric mRNA between the deletion and the inversion types.

It is inferred, therefore, that the duplication type simply increases *CYP19A1* transcription in native *CYP19A1*-expressing tissues, whereas the deletion and the inversion types cause relatively mild and severe *CYP19A1* overexpression in a range of tissues, respectively. These notions would grossly explain why clinical features of affected males and carrier females and endocrine profiles of affected males are apparently milder in the duplication and the deletion types than in the inversion type and why clinical findings were ameliorated with 1 mg/d of anastrozole in the duplication and the deletion types and with 2–4 mg/d of anastrozole in the inversion type. In addition, the different expression pattern between *CYP19A1* and *DMXL2* may explain, in terms of autocrine and/or paracrine effects, why phenotypic features such as gynecomastia tended to be more severe in the deletion type than in the duplication type under similar endocrine profiles.

Furthermore, several findings are notable in this study. First, a similar degree of FSH-dominant hypogonadotropic hypogonadism is present in the three types, with no amelioration of FSH responses to GnRH stimulation after GnRH priming in two cases with the duplication. This suggests that a relatively mild excess of circulatory estrogens, as observed in the duplication and the deletion types, can exert a strong negative feedback effect on FSH secretion, primarily at the pituitary, as has been suggested previously (15–19). Second, although basal T values appear to be mildly and similarly compromised in the three types, age-matched comparison suggests that T responses to hCG stimulation are apparently normal in the duplication and the deletion types and somewhat low in the inversion type. These data, although they remain fragmentary, would primarily be compatible with fairly preserved LH secretion in the three types and markedly increased estrogen values in the inversion type because T production is under the control of LH (1), and excessive estrogens compromise testicular steroidogenic enzyme activity (20, 21). Lastly, although testis volume appears somewhat small, fertility (spermatogenesis) is normally preserved in the three types. This would be consistent with the FSH-dominant hypogonadotropic hypogonadism because FSH plays only a minor role in male fertility (spermatogenesis) (22). Indeed, males with mutations of *FSHR* encoding FSH receptor as well as mice lacking *FSHB* or *FSHR* can be fertile (23, 24).

The results of this study are contrastive to those of the previous studies. In the previous studies, inversions only have been identified, and each inversion is specific to each family or patient (8). By contrast, in this study, the identical duplication was found in two Japanese families A and B, and the same deletion (subtype 2 in Fig. 5) was shared by three Japanese and one Caucasian families D–F, despite apparent nonconsanguinity. This may be explained by assuming that patients with severe phenotype were preferentially examined in the previous studies, whereas those with the AEXS phenotype were analyzed in this study without ascertainment bias. Furthermore, because phenotypes are milder in the duplication and the deletion types than in the inversion type, this may have permitted the spread of the duplication and the deletion types, but not the inversion type, as the founder abnormalities. This notion predicts that the duplication and the deletion types would be identified by examining patients with mild AEXS phenotype.

In summary, the present study shows that AEXS can be caused by duplications of the physiological promoters and microdeletions of the upstream regions of *CYP19A1* and that phenotypic severity is primarily determined by the tissue expression pattern of *CYP19A1* and the chimeric genes and by structural properties of the fused exons. Most importantly, the present study provides novel models for the gain-of-function mutations leading to human genetic disease.

Acknowledgments

Address all correspondence and requests for reprints to: Dr. Tsutomu Ogata, Department of Molecular Endocrinology, National Research Institute for Child Health and Development, 2-10-1 Ohkura, Setagaya, Tokyo 157-8535, Japan. E-mail: tomogata@nch.go.jp.

Present address for T.O.: Department of Pediatrics, Hamamatsu University School of Medicine, Hamamatsu 431-3192, Japan.

This work was supported by Grants for Research on Intractable Diseases (H22-035 and H22-098) from the Ministry of Health, Labor, and Welfare; Grants-in-Aid for Scientific Research (B) (20390265) and (S) (22227002) from the Japan Society for the Promotion of Science; and Grant-in-Aid for Scientific Research on Innovative Areas (22132004) from the Ministry of Education, Culture, Sports, Science, and Technology.

Disclosure Summary: The authors have nothing to declare.

References

1. **Bhasin S** 2008 Testicular disorders. In: Kronenberg HM, Melmed M, Polonsky KS, Larsen PR, eds. Williams textbook of endocrinology. 11th ed. Philadelphia: Saunders; 645–699
2. **Bulun SE, Takayama K, Suzuki T, Sasano H, Yilmaz B, Sebastian S**

2004 Organization of the human aromatase p450 (CYP19) gene. Semin Reprod Med 22:5–9
3. **Demura M, Reierstad S, Innes JE, Bulun SE** 2008 Novel promoter I. 8 and promoter usage in the CYP19 (aromatase) gene. Reprod Sci 15:1044–1053
4. **Harada N, Utsumi T, Takagi Y** 1993 Tissue-specific expression of the human aromatase cytochrome P-450 gene by alternative use of multiple exons 1 and promoters, and switching of tissue-specific exons 1 in carcinogenesis. Proc Natl Acad Sci USA 90:11312–11316
5. **Shozu M, Sebastian S, Takayama K, Hsu WT, Schultz RA, Neely K, Bryant M, Bulun SE** 2003 Estrogen excess associated with novel gain-of-function mutations affecting the aromatase gene. N Engl J Med 348:1855–1865
6. **Binder G, Iliev DI, Dufke A, Wabitsch M, Schweizer R, Ranke MB, Schmidt M** 2005 Dominant transmission of prepubertal gynecomastia due to serum estrone excess: hormonal, biochemical, and genetic analysis in a large kindred. J Clin Endocrinol Metab 90: 484–492
7. **Martin RM, Lin CJ, Nishi MY, Billerbeck AE, Latronico AC, Russell DW, Mendonca BB** 2003 Familial hyperestrogenism in both sexes: clinical, hormonal, and molecular studies of two siblings. J Clin Endocrinol Metab 88:3027–3034
8. **Demura M, Martin RM, Shozu M, Sebastian S, Takayama K, Hsu WT, Schultz RA, Neely K, Bryant M, Mendonca BB, Hanaki K, Kanzaki S, Rhoads DB, Misra M, Bulun SE** 2007 Regional rearrangements in chromosome 15q21 cause formation of cryptic promoters for the CYP19 (aromatase) gene. Hum Mol Genet 16:2529–2541
9. **Tiulpakov A, Kalintchenko N, Semitcheva T, Polyakov A, Dedov I, Sverdlova P, Kolesnikova G, Peterkova V, Rubtsov P** 2005 A potential rearrangement between CYP19 and TRPM7 genes on chromosome 15q21.2 as a cause of aromatase excess syndrome. J Clin Endocrinol Metab 90:4184–4190
10. **Stratakis CA, Vottero A, Brodie A, Kirschner LS, DeAtkine D, Lu Q, Yue W, Mitsiades CS, Flor AW, Chrousos GP** 1998 The aromatase excess syndrome is associated with feminization of both sexes and autosomal dominant transmission of aberrant P450 aromatase gene transcription. J Clin Endocrinol Metab 83:1348–1357
11. **Bellino FL, Osawa Y** 1977 Localization of estrogen synthetase in the chorionic villus fraction after homogenization of human term placenta. J Clin Endocrinol Metab 44:699–707
12. **Kuzmiak HA, Maquat LE** 2006 Applying nonsense-mediated mRNA decay research to the clinic: progress and challenges. Trends Mol Med 12:306–316
13. **Gu W, Zhang F, Lupski JR** 2008 Mechanisms for human genomic rearrangements. Pathogenetics 1:4
14. **Castillo-Davis CI, Mekhedov SL, Hartl DL, Koonin EV, Kondrashov FA** 2002 Selection for short introns in highly expressed genes. Nat Genet 31:415–418
15. **Shaw ND, Histed SN, Srouji SS, Yang J, Lee H, Hall JE** 2010 Estrogen negative feedback on gonadotropin secretion: evidence for a direct pituitary effect in women. J Clin Endocrinol Metab 95:1955–1961
16. **Belgorosky A, Guercio G, Pepe C, Saraco N, Rivarola MA** 2009 Genetic and clinical spectrum of aromatase deficiency in infancy, childhood and adolescence. Horm Res 72:321–330
17. **Alexander DC, Miller WL** 1982 Regulation of ovine follicle-stimulating hormone β-chain mRNA by 17β-estradiol *in vivo* and *in vitro*. J Biol Chem 257:2282–2286
18. **Mercer JE, Clements JA, Funder JW, Clarke IJ** 1988 Luteinizing hormone-β mRNA levels are regulated primarily by gonadotropin-releasing hormone and not by negative estrogen feedback on the pituitary. Neuroendocrinology 47:563–566
19. **Raven G, de Jong FH, Kaufman JM, de Ronde W** 2006 In men, peripheral estradiol levels directly reflect the action of estrogens at the hypothalamo-pituitary level to inhibit gonadotropin secretion. J Clin Endocrinol Metab 91:3324–3328
20. **Moger WH** 1980 Direct effects of estrogens on the endocrine function of the mammalian testis. Can J Physiol Pharmacol 58:1011–1022
21. **Strauss L, Kallio J, Desai N, Pakarinen P, Miettinen T, Gylling H, Albrecht M, Mäkelä S, Mayerhofer A, Poutanen M** 2009 Increased exposure to estrogens disturbs maturation, steroidogenesis, and cholesterol homeostasis via estrogen receptor α in adult mouse Leydig cells. Endocrinology 150:2865–2872
22. **Kumar TR, Wang Y, Lu N, Matzuk MM** 1997 Follicle stimulating hormone is required for ovarian follicle maturation but not male fertility. Nat Genet 15:201–204
23. **Tapanainen JS, Aittomäki K, Min J, Vaskivuo T, Huhtaniemi IT** 1997 Men homozygous for an inactivating mutation of the follicle-stimulating hormone (FSH) receptor gene present variable suppression of spermatogenesis and fertility. Nat Genet 15:205–206
24. **Layman LC, McDonough PG** 2000 Mutations of follicle stimulating hormone-β and its receptor in human and mouse: genotype/phenotype. Mol Cell Endocrinol 161:9–17

CLINICAL GENETICS An International Journal of Genetics, Molecular and Personalized Medicine

Clin Genet 2011: 80: 478–483
Printed in Singapore. All rights reserved

CLINICAL GENETICS
doi: 10.1111/j.1399-0004.2010.01599.x

Short Report

Maternal uniparental isodisomy and heterodisomy on chromosome 6 encompassing a *CUL7* gene mutation causing 3M syndrome

Sasaki K, Okamoto N, Kosaki K, Yorifuji T, Shimokawa O, Mishima H, Yoshiura K-i, Harada N. Maternal uniparental isodisomy and heterodisomy on chromosome 6 encompassing a *CUL7* gene mutation causing 3M syndrome.
Clin Genet 2011: 80: 478–483. © John Wiley & Sons A/S, 2010

We report a case of segmental uniparental maternal hetero- and isodisomy involving the whole of chromosome 6 (mat-hUPD6 and mat-iUPD6) and a cullin 7 (*CUL7*) gene mutation in a Japanese patient with 3M syndrome. 3M syndrome is a rare autosomal recessive disorder characterized by severe pre- and postnatal growth retardation that was recently reported to involve mutations in the *CUL7* or obscurin-like 1 (*OBSL1*) genes. We encountered a patient with severe growth retardation, an inverted triangular gloomy face, an inverted triangle-shaped head, slender long bones, inguinal hernia, hydrocele testis, mild ventricular enlargement, and mild mental retardation. Sequence analysis of the *CUL7* gene of the patient revealed a homozygous missense mutation, c.2975G>C. Genotype analysis using a single nucleotide polymorphism array revealed two mat-hUPD and two mat-iUPD regions involving the whole of chromosome 6 and encompassing *CUL7*. 3M syndrome caused by complete paternal iUPD of chromosome 6 involving a *CUL7* mutation has been reported, but there have been no reports describing 3M syndrome with maternal UPD of chromosome 6. Our results represent a combination of iUPDs and hUPDs from maternal chromosome 6 involving a *CUL7* mutation causing 3M syndrome.

Conflict of interest

None of the authors of this paper declares a conflict of interest.

K Sasaki[a], N Okamoto[b], K Kosaki[c], T Yorifuji[d], O Shimokawa[e], H Mishima[a], K-i Yoshiura[a] and N Harada[e]

[a]Department of Human Genetics, Nagasaki University Graduate School of Biomedical Sciences, Nagasaki, Japan, [b]Osaka Medical Center and Research Institute for Maternal and Child Health, Osaka, Japan, [c]Department of Pediatrics, Keio University School of Medicine, Tokyo, Japan, [d]Department of Pediatric Endocrinology and Metabolism, Children's Medical Center, Osaka City General Hospital, Osaka, Japan, and [e]Cytogenetic Testing Group B, Advanced Medical Science Research Center, Mitsubishi Chemical Medience Corporation, Nagasaki, Japan

Key words: 3M syndrome – cullin 7 (*CUL7*) – Genome-Wide Human SNP Array 6.0 (SNP6.0) – maternal uniparental disomy of chromosome 6 (matUPD6)

Corresponding author: Dr Koh-ichio Yoshiura, Department of Human Genetics, Nagasaki University Graduate School of Biomedical Sciences, Sakamoto 1-12-4, Nagasaki 852-8523, Japan.
Tel.: +81 95 819 7118;
fax: +81 95 849 7121;
e-mail: kyoshi@nagasaki-u.ac.jp

Received 10 September 2010, revised and accepted for publication 12 November 2010

3M syndrome is a rare inherited autosomal recessive disorder characterized by pre- and postnatal growth retardation, characteristic facial features, and skeletal anomalies. Clinical features of 3M syndrome include large head circumference, broad forehead, a triangular facial outline, dolichocephaly, long philtrum, short stature, short thorax and neck, tall vertebral bodies, and slender

long bones and ribs. Males with 3M syndrome occasionally have hypogonadism and hypospadias (1–9). However, intelligence is unaffected and karyotype is normal on conventional chromosome analysis.

In patients with 3M syndrome, disease-causing mutations have been identified in the cullin 7 (*CUL7*, MIM *609577) and obscurin-like 1 (*OBSL1*, MIM *610991) genes (7–9). Mutations of *CUL7* are the major cause of 3M syndrome, accounting for 80% of previously reported cases, whereas *OBSL1* accounts for 20% of cases (8, 10).

Uniparental disomy (UPD) is the transmission pattern of either two copies of the identical chromosome (uniparental isodisomy; iUPD) or of both homologous chromosomes (uniparental heterodisomy; hUPD) from one parent with no contribution from the other parent (11). Phenotypes that are clinically associated with paternal UPD of chromosome 6 (patUPD6) and genomic imprinting have been established, but because of the rarity of maternal UPD of chromosome 6 (matUPD6), clinical features have not yet been established. Here, we report a patient with a homozygous mutation in *CUL7* due to a maternal iUPD of chromosome 6 (mat-iUPD6).

Materials and methods

Clinical report

A Japanese male patient with 3M syndrome was examined in this study. The patient was delivered by caesarean section at 36 weeks of gestation without a family history of 3M syndrome (Fig. 1a). His birth weight was 1000 g (−4.8 SD), length 33.0 cm (−6.8 SD), head circumference 30.2 cm (−1.5 SD), and Apgar score 7/9. Feeding difficulty was noted during the neonatal period. He remained in a neonatal intensive care unit for 2 months and was referred to our group because of developmental delay and muscle hypotonia at 4 months. The patient displayed anomalies including hypospadias, inguinal hernia, hydrocele testis, inverted triangular gloomy face, malar hypoplasia, long eyelashes, epicanthal folds, short nose, anteverted nares, full lips, long philtrum, pointed chin, short chest, grooved lower anterior thorax, hypermobility of joints, and slender long bones (Fig. 1a,b). Mild ventricular enlargement was observed by neuroradiological studies. His growth was severely retarded.

At 2 years 9 months, his height, weight, and head circumference were 69.3 cm (−4.6 SD), 6.8 kg (−6.7 SD), and 48 cm (−1.2 SD), respectively. His head size was disproportionately large compared to his height. Thus the patient was diagnosed as suffering from 3M syndrome. He could understand simple sentences, but could not speak nor sit alone. Partial growth hormone (GH) deficiency was noted. GH replacement therapy was started from 2 years. GH was effective without side effects. At 5 years, his height and weight were 84.8 cm (−5.9 SD) and 10 kg (−3 SD), respectively. He was moderately mentally retarded.

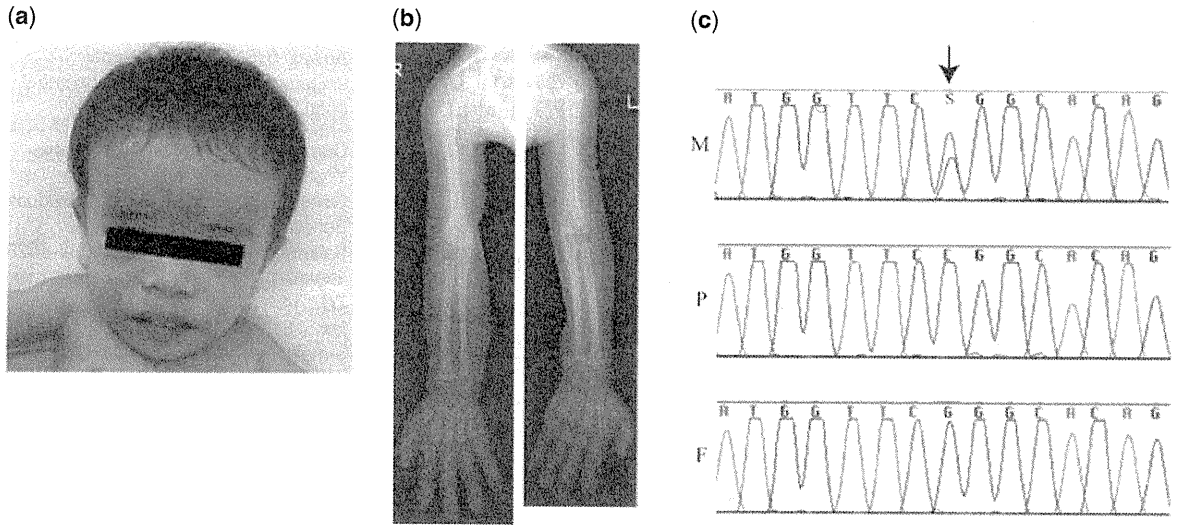

Fig. 1. Facial and skeletal features of the patient at 2 years 7 months of age. (**a**) Note the inverted triangular gloomy face, short nose, full lips, and long philtrum. (**b**) Note the slender long bones. (**c**) Electropherograms of the patient and parents. DNA sequence showing a single base change substituting cytosine for guanine, which results in p.R992P, in the patient. M, mother; P, patient; and F, father.

Conventional cytogenetic studies and FISH analysis

We obtained blood samples under written informed consent for participation in this study. Conventional cytogenetic examination of G-banded chromosomes from peripheral blood lymphocytes was performed. We also performed fluorescence *in situ* hybridization (FISH) analysis on lymphocyte metaphase spreads from the patient using two Bacterial Artificial Chromosome (BAC) clones containing *CUL7*, RP11-628J2 and RP11-653G5, as probes.

Genomic sequencing

Genomic DNA was extracted from peripheral blood following standard protocols. For mutation analysis, we designed primers to amplify all the coding exons of *CUL7* and the flanking intron sequences. Direct sequencing was carried out using a BigDye Terminator v3.1 Cycle sequencing Kit™ and separated on a Genetic Analyzer 3130*xl* (Applied Biosystems Inc., Foster City, CA). Sequence electropherograms were aligned with SEQUENCHER™ software (Gendcodes, Ann Arbor, MI) to visually inspect base alterations.

Microarray analysis

We performed genome-wide single nucleotide polymorphism (SNP) genotyping using Genome-Wide Human SNP Array 6.0 (SNP6.0) following the manufacturer's instructions (Affymetrix, Santa Clara, CA, http://www.affymetrix.com/index.affx). The data generated from Genotyping Console (GTC) 4.0 were loaded into CHROMOSOME ANALYSIS SUITE (CHAS) 1.0.1 software to display the results. We carried out UPD analyses of the patient using genotype data in trio. Genomic positions of SNPs corresponded to the March 2006 human genome (hg18).

Results

Genomic sequencing

We sequenced all 26 coding exons and flanking intronic regions of the *CUL7* gene, which spans a genomic region of approximately 16.3 kb, in the family. In the patient, we detected a homozygous missense mutation (c.2975G>C) in exon 15, which resulted in the substitution of proline for arginine at amino acid residue 992 (p.R992P) (Fig. 1c). The mother was a heterozygous carrier of the mutation, whereas the father was homozygous for the wild-type allele (Fig. 1c). The p.R992P mutation was not detected in 100 unrelated control individuals.

Conventional and molecular cytogenetic analyses

G-banding and FISH analysis at the *CUL7* locus showed a normal karyotype in the patient and the parents with no microdeletion at *CUL7* locus in the patient (data not shown).

Microarray analysis

To confirm paternity, and to find a small size deletion, we performed SNP6.0 analysis. However, no copy number variations (CNVs) were identified in the region containing both *CUL7* and *OBSL1* genes (Fig. 2a). The other variants overlap with reported regions of CNVs in the Database of Genomic Variants (http://projects.tcag.ca/variation) or were transmitted from the parents (data not shown).

To confirm matUPD6 in the patient, we examined the genotypes of the patient/father/mother trio. The results using informative markers indicated that there were two maternal heterodisomic regions (hUPD6-1 and hUPD6-2) and two maternal isodisomic regions (iUDP6-1 and iUPD6-2) in chromosome 6, respectively (Fig. 2 and Table 1). The results indicated that the patient had inherited two alleles from his mother, but none from his father, in chromosome 6. The final karyotype of this patient was 46,XY,upd(6)mat and arr 6p25.3p22.3(110,391–16,287,166)×2 htz mat,6p 22.3q12(16,290,223–65,796,893)×2 hmz mat,6q 12q25.1(65,799,990–150,517,779)×2 htz mat,6q 25.1q27(150,518,012–170,759,956)×2 hmz mat.

Discussion

We identified a causative homozygous mutation in *CUL7* in a patient with 3M syndrome. The results clearly indicate that mat-iUPD6 involving a mutant allele of the *CUL7* gene caused 3M syndrome in the patient.

matUPD6 is relatively rare and seven cases have been reported. The first case was a renal transplant patient who showed growth retardation at birth and mat-iUPD6 (12). The second case was a patient with congenital adrenal hyperplasia (CAH) resulting from a homozygous mutation in the 21-hydroxylase gene (*CYP21*), and had intrauterine growth retardation (IUGR) and mat-iUPD6 (13). The third case was a macerated male fetus from a pregnancy terminated at 23 weeks of gestation because of intrauterine death. The patient showed a mosaic trisomy 6 (14). The fourth case was a male patient with two clinical phenotypes, Klinefelter's syndrome and CAH. His karyotype was mosaic 48,XXY, +mar[30]/47,XXY[20] and

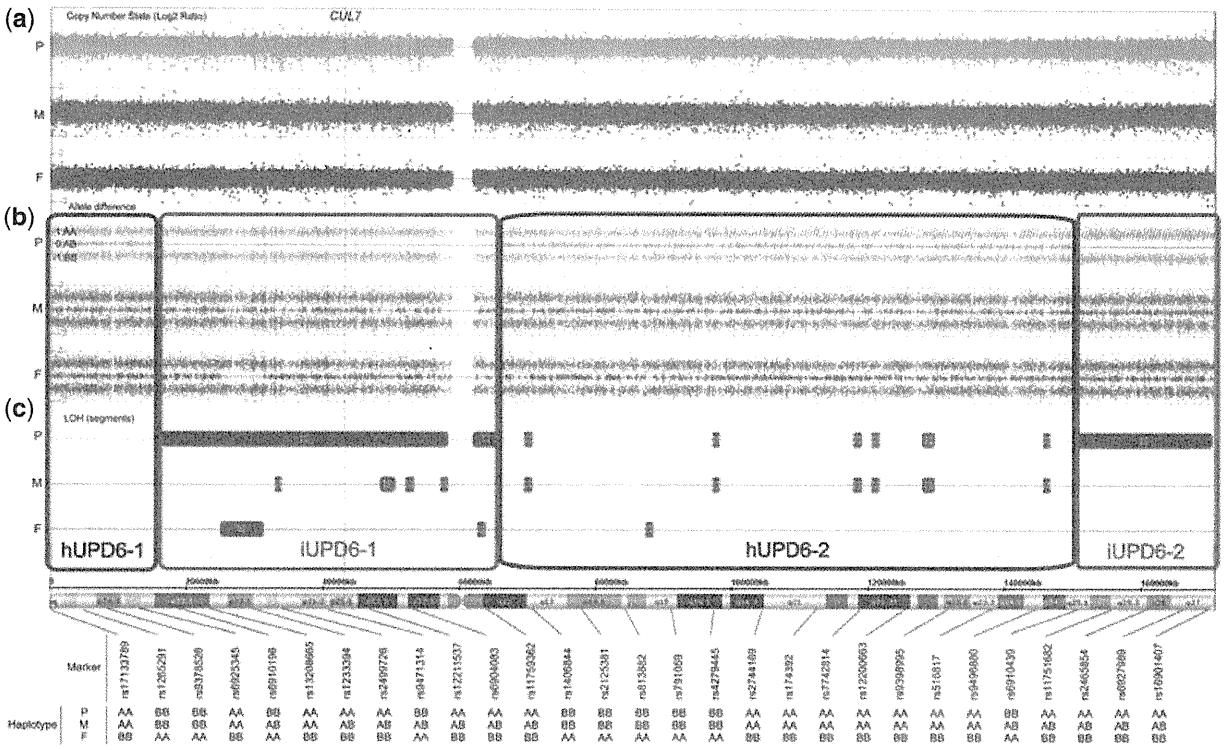

Fig. 2. SNP6.0 data. (**a**) Plots of the SNP6.0 data displayed in ChAS 1.0.1 showing the log2 ratio plot of copy number state, allele difference plot, and loss of heterozygosity (LOH) segment (purple box) (P, patient; M, mother; and F, father). (**b**) The allele difference graph represents the genotypes for each individual single nucleotide polymorphism (SNP). Dots with a value of 1, −1, and 0 represent SNPs with AA, BB, and AB genotypes, respectively. A vertical dashed line indicates the *CUL7* locus. (**c**) The LOH segment plot indicates nine LOH regions on chromosome 6. iUPD6-1 and iUPD6-2 denote the regions of uniparental isodisomy (red box). hUPD6-1 and hUPD6-2 denote the regions of uniparental heterodisomy (blue box). The genotypes on chromosome 6 indicate maternal heterodisomy or isodisomy in the affected offspring [only the uniparental disomy (UPD) markers are displayed].

Table 1. Examination of SNPs from a patient/father/mother trio[a]

			hUPD6-1	iUPD6-1	hUPD6-2	iUPD6-2
Genotype of trio (patient/father/mother)	iUPD	AA/BB/AB	0	534	0	318
		BB/AA/AB	0	576	3	304
	iUPD or hUPD	AA/BB/AA	178	543	605	272
		BB/AA/BB	196	506	563	262
Share genotype (patient/mother)	iUPD or hUPD	AA/AA	2,812	5,897	9,716	3,009
		BB/BB	2,799	5,785	9,557	2,919
	hUPD	AB/AB	1,699	19	6,384	12
		Total of share genotype	7,310	11,701	25,657	5,940
		Share genotype rate (%)	99.82	78.20	99.89	73.31
		Total SNP probe	7,323	14,963	25,684	8,103
		Start SNP	rs4959515	rs9370869	rs9354209	rs9384189
		Start position	110,391	16,290,223	65,799,990	150,518,012
		End SNP	rs9477050	rs9453156	rs7765984	rs6931065
		End position	16,287,166	65,796,893	150,517,779	170,759,956
		Size (bp)	16,176,776	49,506,671	84,717,790	20,241,945
		Cytoband	p25.3-p22.3	p22.3-q12	q12-q25.1	q25.1-q27

hUPD, uniparental heterodisomy; iUPD, uniparental isodisomy; iUPD or hUPD, UPD could not be defined as isodisomy or heterodisomy; SNP, single nucleotide polymorphism.

[a]Each row contains information on each matUPD6 inheritance block identified by trio haplotype analysis.

both the X chromosome and chromosome 6 showed maternal iUPD. This case also was notable for IUGR and growth retardation at 8 months of age (15). The fifth case was a fetus with IUGR at 29 weeks of pregnancy from a 45-year-old patient. The case was ascertained as trisomy 6 mosaicism in cultured chorionic villi but disomy in amniocytes; analysis of DNA markers in amniocytes and parental samples revealed mat-iUPD6 in disomy cells (16). The sixth case was a male infant with molybdenum cofactor deficiency who showed developmental delay. SNP analysis with the trio revealed that at least 6p21.1-6p24.3 were mat-iUPD6, but not another region were remain unclear (17). The seventh case was a patient with cleft lip and palate, and showed a complete maternal hUPD on chromosome 6 (mat-hUPD6). This case had no notable IUGR in the serial ultrasound examination (18). Taken together, IUGR and growth retardation were found in the cases with mat-iUPD6 (12, 13, 15–17), while these were not found in cases with mat-hUPD6 (14, 18). The IUGR and growth retardation in cases of mat-iUPD6 may be the result of homozygosity of chromosome 6. On the basis of these reports, no clear maternal imprinting effect of chromosome 6 can be established; however, recently, a complete gain of methylation phenotype at insulin-like growth factor 2 receptor was shown in patients with growth restriction (19).

The patient with homozygous mutation in *CUL7* and matUPD6 had clinical features compatible with 3M syndrome. However, the patient displayed certain features that have not been previously reported among patients with *CUL7* mutations such as mild mental retardation, inguinal hernia, hydrocele testis, and mild ventricular enlargement (7, 8, 20). Mild mental retardation is an especially characteristic phenotype in our case because most patients with 3M syndrome have normal intelligence. It is difficult to determine whether matUPD6 had a significant role in the development of certain feature in our case.

Here we report a case of 3M syndrome with a homozygous mutation that resulted from maternal iUPD, including the *CUL7* gene. Although complete paternal or maternal UPD for chromosome 6 has previously been reported, this is the first report of a patient with 3M syndrome who has a mixture of mat-hUPD6 and mat-iUPD6 regions. Our results emphasize that UPD should be considered possible mechanism for developing the autosomal recessive disorders including 3M syndrome.

Acknowledgements

We are grateful to the patient and his parents for their participation in this research. We also thank Ms Miho Ooga and Ms Chisa Hayashida for technical assistance. K.-I. Y. was supported in part by Grants-in-Aid for Scientific Research from the Ministry of Health, Labour and Welfare, and in part by the Takeda Scientific Foundation and the Naito Foundation.

References

1. Winter RM, Baraitser M, Grant DB, Preece MA, Hall CM. The 3-M syndrome. J Med Genet 1984: 21: 124–128.
2. Feldmann M, Gilgenkrantz S, Parisot S, Zarini G, Marchal C. 3M dwarfism: a study of two further sibs. J Med Genet 1989: 26 (9): 583–585.
3. García-Cruz D, Cantú JM. Heterozygous expression in 3-M slender-boned nanism. Hum Genet 1979: 52: 221–226.
4. Mueller RF, Buckler J, Arthur R et al. The 3-M syndrome: risk of intracerebral aneurysm? J Med Genet 1992: 29: 425–427.
5. Le Merrer M, Brauner R, Maroteaux P. Dwarfism with gloomy face: a new syndrome with features of 3-M syndrome. J Med Genet 1991: 28: 186–191.
6. Spranger J, Opitz JM, Nourmand A. A new familial intrauterine growth retardation syndrome the "3-M syndrome". Eur J Pediatr 1976: 123: 115–124.
7. Huber C, Dias-Santagata D, Glaser A et al. Identification of mutations in *CUL7* in 3-M syndrome. Nat Genet 2005: 37: 1119–1124.
8. Huber C, Delezoide AL, Guimiot F et al. A large-scale mutation search reveals genetic heterogeneity in 3M syndrome. Eur J Hum Genet 2009: 17: 395–400.
9. Hanson D, Murray PG, Sud A et al. The primordial growth disorder 3-M syndrome connects ubiquitination to the cytoskeletal adaptor *OBSL1*. Am J Hum Genet 2009: 84: 801–806.
10. Huber C, Fradin M, Edouard T et al. OBSL1 mutations in 3-M syndrome are associated with a modulation of IGFBP2 and IGFBP5 expression levels. Hum Mutat 2010: 31: 20–26.
11. Engel E. A new genetic concept: uniparental disomy and its potential effect, isodisomy. Am J Med Genet 1980: 6: 137–143.
12. van den Berg-Loonen EM, Savelkoul P, van Hooff H, van Eede P, Riesewijk A, Geraedts J. Uniparental maternal disomy 6 in a renal transplant patient. Hum Immunol 1996: 45: 46–51.
13. Spiro RP, Christian SL, Ledbetter DH et al. Intrauterine growth retardation associated with maternal uniparental disomy for chromosome 6 unmasked by congenital adrenal hyperplasia. Pediatr Res 1999: 46: 510–513.
14. Cockwell AE, Baker SJ, Connarty M, Moore IE, Crolla JA. Mosaic trisomy 6 and maternal uniparental disomy 6 in a 23-week gestation fetus with atrioventricular septal defect. Am J Med Genet A 2006: 140: 624–627.
15. Parker EA, Hovanes K, Germak J, Porter F, Merke DP. Maternal 21-hydroxylase deficiency and uniparental isodisomy of chromosome 6 and X results in a child with 21-hydroxylase deficiency and Klinefelter syndrome. Am J Med Genet A 2006: 140: 2236–2240.
16. Haag M, Beischel L, Rokeach J et al. First prenatal detection of maternal uniparental disomy (UPD) of chromosome 6 and 'rescue' of trisomy 6 [abstract]. *Abstracts of the 57th Annual Meeting of the ASHG 2007*; Abstract no 2428.
17. Gümüş H, Ghesquiere S, Per H et al. Maternal uniparental isodisomy is responsible for serious molybdenum cofactor deficiency. Dev Med Child Neurol 2010: 52 (9): 868–872.

18. Salahshourifar I, Halim AS, Sulaiman WA, Zilfalil BA. Maternal uniparental heterodisomy of chromosome 6 in a boy with an isolated cleft lip and palate. Am J Med Genet A 2010: 152A (7): 1818–1821.
19. Turner CL, Mackay DM, Callaway JL et al. Methylation analysis of 79 patients with growth restriction reveals novelpatterns of methylation change at imprinted loci. Eur J Hum Genet 2010: 18: 648–655.
20. Maksimova N, Hara K, Miyashia A et al. Clinical, molecular and histopathological features of short stature syndrome with novel *CUL7* mutation in Yakuts: new population isolate in Asia. J Med Genet 2007: 44: 772–778.

CLINICAL REPORT

AMERICAN JOURNAL OF medical genetics PART A

A De Novo Deletion of 20q11.2–q12 in a Boy Presenting With Abnormal Hands and Feet, Retinal Dysplasia, and Intractable Feeding Difficulty

Yoko Hiraki,[1,2] Akira Nishimura,[2] Michiko Hayashidani,[3] Yoshiko Terada,[4] Gen Nishimura,[5] Nobuhiko Okamoto,[6] Sachiko Nishina,[7] Yoshinori Tsurusaki,[2] Hiroshi Doi,[2] Hirotomo Saitsu,[2] Noriko Miyake,[2] and Naomichi Matsumoto[2]*

[1]Hiroshima Municipal Center for Child Health and Development, Hiroshima, Japan

[2]Department of Human Genetics, Yokohama City University Graduate School of Medicine, Yokohama, Japan

[3]Medical Center for Premature and Neonatal Infants, Hiroshima City Hospital, Hiroshima, Japan

[4]Department of Ophthalmology, Hiroshima City Hospital, Hiroshima, Japan

[5]Department of Pediatric Imaging, Tokyo Metropolitan Children's Medical Center, Tokyo, Japan

[6]Department of Medical Genetics, Osaka Medical Center and Research Institute for Maternal and Child Health, Osaka, Japan

[7]Department of Ophthalmology, National Center for Child Health and Development, Tokyo, Japan

Received 18 June 2010; Accepted 23 October 2010

Proximal interstitial deletions involving 20q11–q12 are very rare. Only two cases have been reported. We describe another patient with 20q11.21–q12 deletion. We precisely mapped the 6.5-Mb deletion and successfully determined the deletion landmarks at the nucleotide level. Common clinical features among the three cases include developmental delay, intractable feeding difficulties with gastroesophageal reflux, and facial dysmorphism including triangular face, hypertelorism, and hypoplastic alae nasi, indicating that the 20q11.2–q12 deletion can be a clinically recognizable syndrome. This is also supported by the fact that the three deletions overlap significantly. In addition, unique features such as arthrogryposis/fetal akinesia (hypokinesia) deformation and retinal dysplasia are recognized in the patient reported herein. © 2011 Wiley-Liss, Inc.

Key words: 20q interstitial deletion; abnormal hands and feet; retinal dysplasia; feeding difficulty

How to Cite this Article:
Hiraki Y, Nishimura A, Hayashidani M, Terada Y, Nishimura G, Okamoto N, Nishina S, Tsurusaki Y, Doi H, Saitsu H, Miyake N, Matsumoto N. 2011. A de novo deletion of 20q11.2–q12 in a boy presenting with abnormal hands and feet, retinal dysplasia, and intractable feeding difficulty.
Am J Med Genet Part A.

INTRODUCTION

Interstitial deletions of the long arm of chromosome 20 are rare. To our knowledge, a total of 12 patients have been reported in the literature [Petersen et al., 1987; Shabtai et al., 1993; Aldred et al., 2002; Genevieve et al., 2005; Callier et al., 2006; Borozdin et al., 2007; Iqbal and Al-Owain, 2007]. Among them, only two cases showed the proximal q deletion (20q11–q12), not extending to q13 [Callier et al., 2006; Iqbal and Al-Owain, 2007]. One patient had a 6.6-Mb deletion at 20q11.21–q11.23 [Callier et al., 2006], and the other [Iqbal and Al-Owain, 2007] showed a 6.8-Mb deletion at 20q11.2–q12. Here, we report on the third patient with a 6.5-Mb deletion at 20q11.21–q12, clinically showing mental retardation, minor craniofacial anomalies, and intractable feeding difficulties. The deletion has been precisely analyzed at the nucleotide level and his detailed clinical manifestations will be presented.

Grant sponsor: Japan Society for the Promotion of Science (JSPS); Grant sponsor: Ministry of Health, Labour and Welfare; Grant sponsor: Ministry of Education, Culture, Sports, Science and Technology of Japan; Grant sponsor: Scientific Research.

*Correspondence to:
Naomichi Matsumoto, Department of Human Genetics, Yokohama City University Graduate School of Medicine, Fukuura 3-9, Kanazawa-ku, Yokohama 236-0004, Japan. E-mail: naomat@yokohama-cu.ac.jp

Published online in Wiley Online Library (wileyonlinelibrary.com).
DOI 10.1002/ajmg.a.33818

CLINICAL REPORT

The 18-month-old boy was the first product of healthy 22-year-old mother and 25-year-old father without any consanguinity. Pregnancy was uneventful. Family history was unremarkable. He was born by spontaneous vaginal delivery at 38 weeks of gestation. Birth weight was 2,230 g (−1.7 SD), length 44.0 cm (−1.9 SD), and OFC 32.5 cm (−0.3 SD). Multiple malformations including patent ductus arteriosus, patency of foramen ovale, and dysmorphic face were noted. He was tube-fed due to poor swallowing and oxygen therapy was required until 4 months because of respiratory disturbance. X-ray examination at age of 1 month revealed small thorax and mild slender long bones. In addition, right eye retinal fold was pointed out. At age of 3 months, upper gastrointestinal tract was investigated because of recurrent vomiting, and gastroesophageal reflux (GER) and esophageal hiatus hernia were found. Esophageal hiatus hernia was alleviated spontaneously, but GER persisted.

At age of 4 months, he was referred to us for evaluation of his developmental delay. He was noted to have the following craniofacial features: triangular face, premature closure fontanelle, slopping forehead, wide bending eyebrows, hypertelorism, low-set and posterior rotated ears, long columella nasi, mild hypoplastic alae nasi, short and well-defined philtrum, thin lips with tucked-in lower lip, submucosal cleft palate, microretrognathia and posterior low hair-line (Fig. 1A,B and Table I). Additionally, abnormal hands and feet were recognized, consisted of restriction of all proximal interphalangeal joints and over-extension of all distal interphalangeal joints of hands and feet, radial deviation of 2nd fingers, clinodactyly of the 2nd and 5th fingers, lack of flexion creases bilaterally, right preaxial polydactyly, left single palmar, and talipes valgus. Mild restriction of elbow, hip and knee joints bilaterally was also noted (Fig. 1C–E and Table I).

At 15 months, his weight was 7.5 kg (−2.3 SD), length 71.8 cm (−2.7 SD), and OFC 44.4 cm (−1.6 SD). He could roll over one side and shift a toy from one hand to the other. Social smile was seen, but he could not recognize his parents (DQ 48). His dysphagia persisted based on the modified swallowing study [Kanda et al., 2005]; he required tube-feeding, and rejected oral intake. Ophthalmic examination at 15 months revealed broom-like pattern of retinal vessels extending from optic disc to periphery with a falciform retinal fold in the right eye, causing visual impairment. In the left eye, mild opacity in the lateral portion of vitreous body was found. These findings led to the diagnosis of bilateral retinal dysplasia. Anterior segment and optic disc were normal. Left hearing loss was suspected by auditory brainstem response, otoacoustic emission, and behavioral observation audiometry. Brain magnetic resonance imaging revealed cortical atrophy and mild ventriculomegaly. Blood biochemistry and abdominal ultrasonographic examination were all normal. Serological TORCH (toxoplasma, rubella, cytomegarovirus, and herpes simplex) testing was negative. At 18 months, the shortening of 5th middle phalanges of fingers and absence of middle phalanges of the toes were confirmed by X-ray examination.

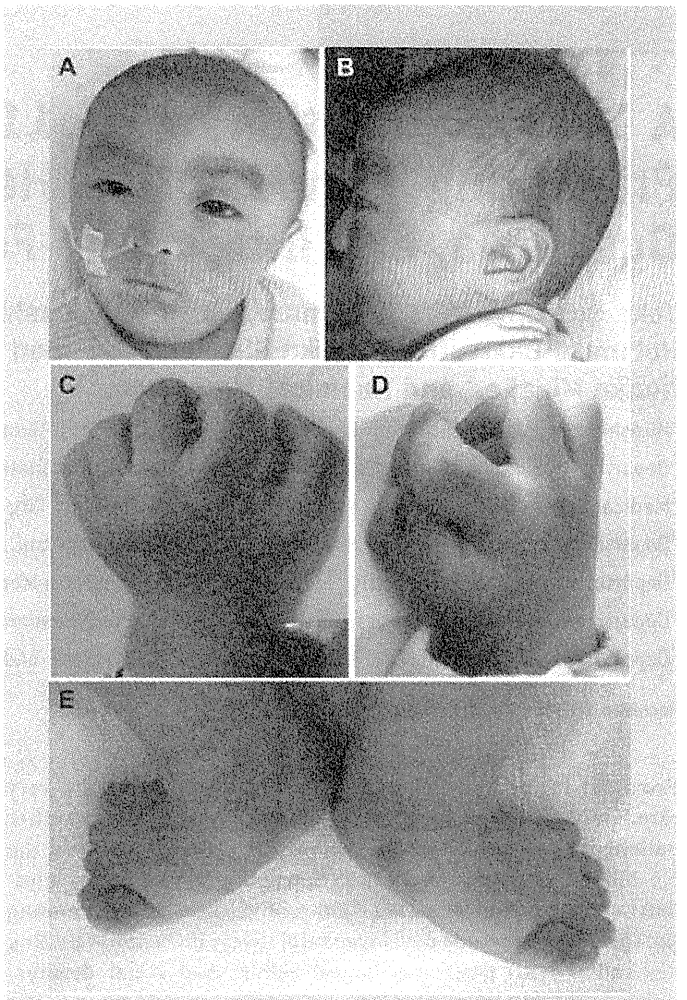

FIG. 1. Photographs of the patient at age of 4 months. A,B: Facial abnormalities including triangular face, wide and bending eyebrows, hypertelorism, long columella, thin lips with tucked-in lower lip, and microretrognathia were recognized. C (left hand) and D (right): Bilateral camptodactyly associated with radial deviation of the 2nd fingers and clinodactyly of the 2nd and 5th, and right preaxial polydactyly were noted. E: Camptodactyly with talipes valgus in both feet.

CYTOGENETIC AND MOLECULAR ANALYSIS

G-banded chromosomal analysis (550 bands level) of the patient's blood lymphocytes indicated normal karyptype (46,XY) (data not shown). Fluorescence in situ hybridization (FISH) analysis using all chromosomal subtelomeric clones did not show any abnormalities. Array CGH analysis using NimbleGen 385K Array (Roche NimbleGen, Inc., Madison, WI) demonstrated a 6.5-Mb heterozygous deletion at 20q11.2–q12 (UCSC genome coordinates 2006 Mar. version, chromosome 20: 31,269,661–37,782,841 bp) (Fig. 2A). The deletion was also confirmed by FISH using BACs (RP11-322B6 and RP11-782C16 at 21q11.21, and RP11-54P22 and RP11-467J15 at 20q12), RP11-787C16 and RP11-54P22 was deleted while RP11-322B6 and RP11-467J15 were not deleted (Fig. 3). The deletion junction was successfully amplified by PCR using primers (Primer A: 5′-TGA TAG AGC CAA CTG GGT CAT GTG C-3′, Primer C: 5′-TCT AGC TTG CTG AAT TCC TGC CTG A-3′) (Fig. 2B) and its product was sequenced. The deleted region was from 31,274,015 to 37,783,826 bp (6,509,811 bp) with 5-bp overlap (ATAGA) (Fig. 2C). The deletion occured de novo as FISH and

TABLE I. Clinical Manifestations of Reported Cases of 20q11–q12 Deletion

	Calliers' case (4 y, female)	Iqbals' case (2 y, male)	Present case (18 m, male)
General			
Growth retardation	+	+	+
Developmental delay	+	+	+
Autistic behavior	+	+	+
Sensory abnormalities/self-injury	+	+	+
Feeding difficulties	+	+	+
Gastroesophageal reflux	+	+	+
Gastrointestinal abnormalities	+ (Pyloric stenosis)	−	+ (Esophageal hiatus hernia)
Feeding intolerance	+ (Diarrhea, vomiting)	−	−
Dysphagia			+
Food refusal	+		+
Muscle tone	Hypertonia	Normal tone except for difficulty in extending the hips	Normal tone
Hearing loss		+	+
Congenital heart defect	−	−	+
Seizure/epilepsy		−	+
Central nervous system			
Cerebral atrophy	+	+	+
Craniofacial			
Triangular face	+	+	+
Hypertelorism	+	+	+
Hypoplastic alae nasi	+	+	+
Sparse hair	+		+
Down-slanting palpebral fissures	+		+
Long columella	+		+
Short, well-defined philtrum	+		+
Thin lips	+		+
Microretrognathia	+		+
Low-set ears	+		+
Extremities			
Arthrogryposis			+
Preaxial polydactyly			+
Clinodactyly of 5th fingers	+		+
Talipes equinovarus		+	
Talopes valgus			+
Ocular			
Retinal dysplasia			+
Microphthalmia		+	−
Duane anomaly		+	n.d.
Strabismus	+		−
Others			
Genital anomlies		+	−

Shadow indicates common features among three cases. y, year(s); m, month(s); +, positive; −, negative; n.d., not determined.

junction PCRs denied the deletion in parental samples (FISH data not shown and Fig. 2B by PCR using primers A, B, and C [primer B: 5′-AGC TGC TCA AAG TGG GGT ATT CTG G-3′]).

DISCUSSION

In this study, we precisely analyzed the 6.5-Mb deletion at 20q11.2–q12 in a boy, presenting with abnormal hands and feet, retinal dysplasia, and intractable feeding difficulty. Proximal interstitial deletions of 20q11–q12 are very rare. Only two cases have been reported and analyzed either by chromosomal CGH and FISH analysis or BAC array CGH with 1-Mb resolution [Callier et al., 2006; Iqbal and Al-Owain, 2007]. Clinical features are presented in Figure 1 and summarized in Table I. Three deletions are overlapping and the shortest region of overlap is from 20q11.22 to q11.23 (Fig. 3). Common clinical features among three cases are

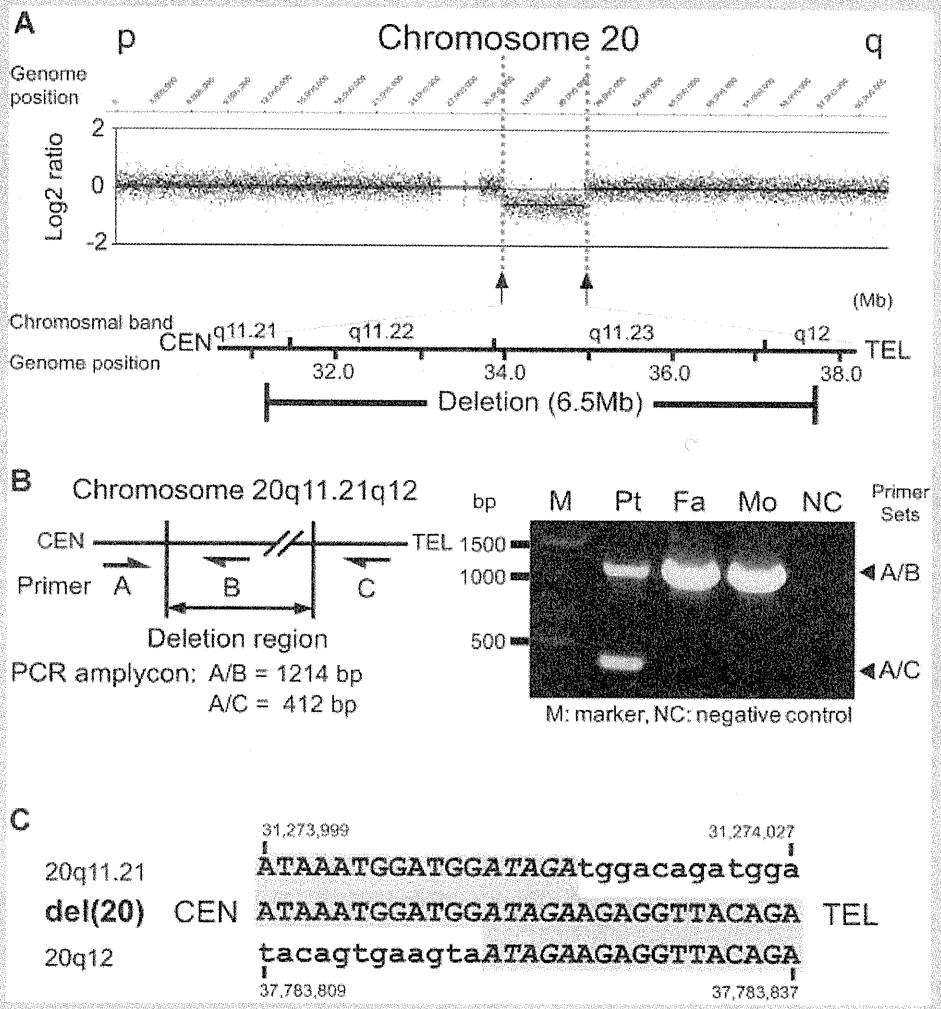

FIG. 2. Analysis of the 20q11.21–q12 deletion. A: High-resolution SNP array revealed the 6.5-Mb deletion at 20q11.21–q12. In the upper part, *Y* and *X* axes indicate probe signal intensity (log 2 ratio) and probe position in chromosome 20, respectively, and in the lower, chromosomal bands together with location of the deletion are shown. B: PCR system (left) to delineate the deletion and its result (right). C: Deletion junction sequence. Upper and lower sequences are normal ones around at proximal [20q11.21] and distal [20q12] deletion breakpoints, respectively. Middle shows the deletion junction in the patient. Gray shadow indicates matched sequences.

growth/developmental retardation, intractable feeding difficulties with GER, cerebral atrophy, and dysmorphic face including triangular face, hypertelorism, and hypoplastic alae nasi. In addition, two out of three patients shared many other facial dysmorphism including sparse hair, downslanting palpebral fissures, long columella, short and well-defined philtrum, thin lips, microretrognathia, and low-set ears. These findings suggest that the 20q11.22–q11.23 deletion can be a recognizable microdeletion syndrome. In addition, unique findings of hands and feet abnormalities as well as retinal dysplasia were found in our patient.

Intractable feeding difficulties in the three patients, is the largest concern for the family, and are speculated to be caused by combined factors: prolonged dysphagia (in our case), aspiration associated with GER (in all three), upper gastrointestinal tract abnormalties (pyloric stenosis [Callier et al., 2006] or esophageal hiatus hernia in our case), vomiting/diarrhea because of feeding intorerance [Callier et al., 2006], sensory abnormalities (in all), and food refusal (in the Callier et al. and our patient).

According to UCSC genome browser (March 2006 assembly), the 6.5-Mb deleted segment identified in our patient encompasses at least 96 known genes, including nine genes related to human disorders. One of these is growth/differentiation factor-5 (*GDF5*, also known as *CDMP1*). This is a protein which belongs to the GDF-subgroup of BMPs and plays an key regulatory role in embryonic skeletal and joint development. *GDF5* abnormalities are known to cause a variety of different skeletal disorders. Interestingly, Everman et al. [2002] and Yang et al. [2008] indicated that functional *GDF5* haploinsufficiency was the culprit of brachydactyly type C (BDC,

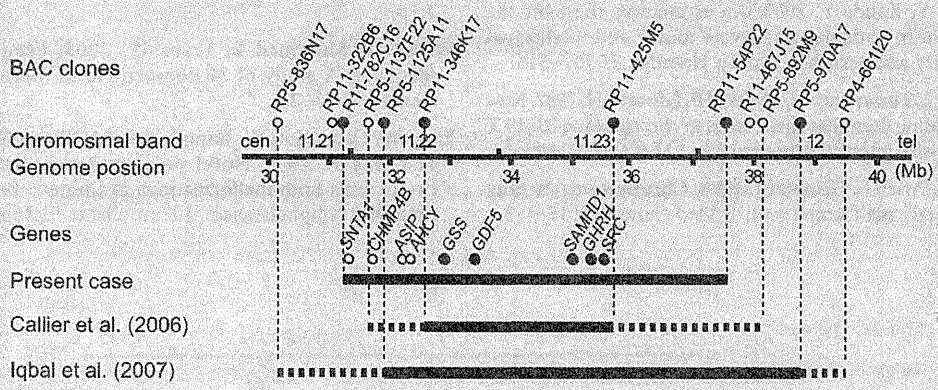

FIG. 3. Shematic presentation of the 20q11–q12 deletions. From top to bottom, BAC clones delineating deletions of all the cases [filled dot: deleted, open dot: not deleted] [Callier et al., 2006; Iqbal and Al-Owain, 2007], chromosomal bands from 20q11.2 to 20q12, genomic position, OMIM genes, and deleted regions of our case and previous ones. Solid and dotted horizontal lines indicate deleted and unconfirmed regions due to the relatively low resolution of the analytical methods.

OMIM #113100) by in vitro studies. As our patient has the *GDF5* haploinsufficiency, he may have the risk for BDC. However, he did not show this manifestation. He did have polydactyly, talipes valgus, and absence of the middle phalanges of the toes, which have been often found in individuals with BDC [Everman et al., 2002; Temtamy and Aglan, 2008]. Our patient did have a fetal akinesia (or hypokinesia) deformation phenotype (FADP). The short neck, hypertelorism, micrognathia, small thorax, postnatal respiratory disturbance, prolonged feeding difficulty, and slender long bone could represent FADP. FADP is a clinically and genetically heterogeneous constellation arising from fetal akinesia or decrease in utero movement due to intrinsic factors including neuropathy, myopathy, and restrictive dermopathy or extrinsic factors that limit fetal movement (e.g., tetragen exposure or fetal crowding) [Witters et al., 2002; Bamshad et al., 2009]. As extrinsic factors (e.g., abnormality of amniotic fluid, fetal crowding, congenital infection, and use of the drug in utero) could not be confirmed in this patient and the arthrogryposis and FADP are accompanied by other organ anomalies and developmental delay, the gene(s) at 20q11.21–q11.23 may be a primary intrinsic cause. Unfortunately, as skeletal malformations in the other two cases having the 20q11.2–q12 deletion were not fully described [Callier et al., 2006; Iqbal and Al-Owain, 2007], it is difficult to discuss the relationship between skeletal features and gene(s) in 20q11.2–q12 deletion.

Retinal dysplasia associated with falciform retinal fold and impaired vision was also noted. Retinal dysplasia is defined as abnormal growth and differentiation of embryonic retina either due to in utero environmental factors such as viral infection, tetragen exposure, retinopathy of prematurity or genetic factors. To our knowledge, this is the first description of retinal dysplasia associated with 20q11.2–q12 deletion.

ACKNOWLEDGMENTS

We are grateful to the patient and his family for their participation and support to this study. Grant-in Aid for Japan Society for the Promotion of Science (JSPS) Fellow (A.N.), Research Grants from the Ministry of Health, Labour and Welfare (N.M.), Grant-in-Aid from the Ministry of Education, Culture, Sports, Science and Technology of Japan (N.M.), and Grant-in-Aid for Scientific Research from JSPS (N.M.).

REFERENCES

Aldred MA, Aftimos S, Hall C, Waters KS, Thakker RV, Trembath RC, Brueton L. 2002. Constitutional deletion of chromosome 20q in two patients affected with albright hereditary osteodystrophy. Am J Med Genet 113:167–172.

Bamshad M, Van Heest AE, Pleasure D. 2009. Arthrogryposis: A review and update. J Bone Joint Surg Am 91:40–46.

Borozdin W, Graham JM Jr, Bohm D, Bamshad MJ, Spranger S, Burke L, Leipoldt M, Kohlhase J. 2007. Multigene deletions on chromosome 20q13.13-q13.2 including SALL4 result in an expanded phenotype of Okihiro syndrome plus developmental delay. Hum Mutat 28:830.

Callier P, Faivre L, Marle N, Thauvin-Robinet C, Sanlaville D, Gosset P, Prieur M, Labenne M, Huet F, Mugneret F. 2006. Major feeding difficulties in the first reported case of interstitial 20q11.22-q12 microdeletion and molecular cytogenetic characterization. Am J Med Genet Part A 140A:1859–1863.

Everman DB, Bartels CF, Yang Y, Yanamandra N, Goodman FR, Mendoza-Londono JR, Savarirayan R, White SM, Graham JM Jr, Gale RP, Svarch E, Newman WG, Kleckers AR, Francomano CA, Govindaiah V, Singh L, Morrison S, Thomas JT, Warman ML. 2002. The mutational spectrum of brachydactyly type C. Am J Med Genet 112:291–296.

Genevieve D, Sanlaville D, Faivre L, Kottler ML, Jambou M, Gosset P, Boustani-Samara D, Pinto G, Ozilou C, Abeguile G, Munnich A, Romana S, Raoul O, Cormier-Daire V, Vekemans M. 2005. Paternal deletion of the GNAS imprinted locus (including Gnasxl) in two girls presenting with severe pre- and post-natal growth retardation and intractable feeding difficulties. Eur J Hum Genet 13:1033–1039.

Iqbal MA, Al-Owain M. 2007. Interstitial del(20)(q11.2q12)—Clinical and molecular cytogenetic characterization. Am J Med Genet Part A 143A:1880–1884.

Kanda T, Murayama K, Kondo I, Kitazumi E, Takahashi K, Nakatani K, Yoneyama A, Yamori Y, Kanda Y. 2005. An estimation chart for the possibility of aspiration in patients with severe motor and intellectual disabilities: Its reliability and accuracy. No To Hattatsu 37:307–316.

Petersen MB, Tranebjaerg L, Tommerup N, Nygaard P, Edwards H. 1987. New assignment of the adenosine deaminase gene locus to chromosome 20q13 X 11 by study of a patient with interstitial deletion 20q. J Med Genet 24:93–96.

Shabtai F, Ben-Sasson E, Arieli S, Grinblat J. 1993. Chromosome 20 long arm deletion in an elderly malformed man. J Med Genet 30:171–173.

Temtamy SA, Aglan MS. 2008. Brachydactyly. Orphanet J Rare Dis 3:15.

Witters I, Moerman P, Fryns JP. 2002. Fetal akinesia deformation sequence: A study of 30 consecutive in utero diagnoses. Am J Med Genet 113:23–28.

Yang W, Cao L, Liu W, Jiang L, Sun M, Zhang D, Wang S, Lo WH, Luo Y, Zhang X. 2008. Novel point mutations in GDF5 associated with two distinct limb malformations in Chinese: Brachydactyly type C and proximal symphalangism. J Hum Genet 53:368–374.

RESEARCH ARTICLE

AMERICAN JOURNAL OF medical genetics PART A

Submicroscopic Deletion in 7q31 Encompassing *CADPS2* and *TSPAN12* in a Child With Autism Spectrum Disorder and PHPV

Nobuhiko Okamoto,[1]* Yoshikazu Hatsukawa,[2] Keiko Shimojima,[3] and Toshiyuki Yamamoto[3]

[1]Department of Medical Genetics, Osaka Medical Center and Research Institute for Maternal and Child Health, Osaka, Japan

[2]Department of Ophthalmology, Osaka Medical Center and Research Institute for Maternal and Child Health, Osaka, Japan

[3]Institute for Integrated Medical Sciences, Tokyo Women's Medical University, Tokyo, Japan

Received 23 August 2010; Accepted 9 March 2011

We performed array comparative genomic hybridization utilizing a whole genome oligonucleotide microarray in a patient with the autism spectrum disorders (ASDs) and persistent hyperplastic primary vitreous (PHPV). Submicroscopic deletions in 7q31 encompassing *CADPS2* (Ca^{2+}-dependent activator protein for secretion 2) and *TSPAN12* (one of the members of the tetraspanin superfamily) were confirmed. The *CADPS2* plays important roles in the release of neurotrophin-3 and brain-derived neurotrophic factor. Mutations in *TSPAN12* are a relatively frequent cause of familial exudative vitreoretinopathy. We speculate that haploinsufficiency of *CADPS2* and *TSPAN12* contributes to ASDs and PHPV, respectively.

Key words: *CADPS2*; *TSPAN12*; autism; PHPV; CGH

How to Cite this Article:
Okamoto N, Hatsukawa Y, Shimojima K, Yamamoto T. 2011. Submicroscopic deletion in 7q31 encompassing *CADPS2* and *TSPAN12* in a child with autism spectrum disorder and PHPV.
Am J Med Genet Part A 155:1568–1573.

INTRODUCTION

Autism spectrum disorders (ASDs OMIM %209850) are complex neurodevelopmental conditions characterized by social communication disabilities, no or delayed language development, and stereotyped and repetitive behaviors. A number of studies have confirmed that genetic factors play an important role in ASDs.

About 10% of ASDs are associated with a Mendelian syndrome (e.g., fragile X syndrome, tuberous sclerosis and Timothy syndrome). Cytogenetic approaches revealed a high frequency of large chromosomal abnormalities (3–7% of patients), including the most frequently observed maternal 15q11-13 duplication (1–3% of patients). Association studies and mutation analysis of candidate genes have implicated the synaptic genes *NLGN3*(Neuroligin3 OMIM*300336), *NLGN4* (OMIM*300427) [Jamain et al., 2003], *SHANK3* (OMIM*606230)[Durand et al., 2007; Moessner et al., 2007], *NRXN1*(Neurexin1 MIM + 600565) [Kim et al., 2008], *SHANK2* (OMIM*603290) [Berkel et al., 2010], and *CNTNAP2* (MIM*604569) [Alarcón et al., 2008; Arking et al., 2008] in ASDs. There is increasing evidence that the *SHANK3-NLGN4-NRNX1* postsynaptic density genes play important roles in the pathogenesis of ASDs.

Recently, on association between de novo copy number variation (CNV) and ASDs was revealed. Sebat et al. [2007] performed comparative genomic hybridization (CGH) on the genomic DNA from ASD patients and unaffected subjects to detect de novo CNV. As a result, they identified CNV in 12 out of 118 (10%) patients with sporadic ASD and confirmed de novo CNV were significantly associated with ASDs. Marshall et al. [2008] performed a genome-wide search for structural abnormalities in 427 unrelated ASD patients using SNP microarray analysis and karyotyping. De novo CNV were found in approximately 7% and approximately 2% of idiopathic families with one ASD child, or two or more ASD siblings, respectively. These authors discovered a CNV at 16p11.2 with an approximate frequency of 1%. Glessner et al. [2009] reported the results from a whole-genome CNV study of many European ASD patients and controls and found several new susceptibility genes encoding neuronal cell-adhesion molecules, including *NLGN1* and *ASTN2*, and genes involved in the ubiquitin pathways, including *UBE3A*, *PARK2*, *RFWD2*, and *FBXO40*. The investigators suggested that two gene networks, neuronal cell-

Grant sponsor: Ministry of Health, Labour and Welfare of Japan.
*Correspondence to:
Nobuhiko Okamoto, Department of Medical Genetics, Osaka Medical Center and Research Institute for Maternal and Child Health, 840 Murodo-cho, Izumi, Osaka 594-1101, Japan. E-mail: okamoto@osaka.email.ne.jp
Published online 27 May 2011 in Wiley Online Library (wileyonlinelibrary.com).
DOI 10.1002/ajmg.a.34028

adhesion and ubiquitin degradation, that are expressed within the central nervous system contribute to the genetic susceptibility of ASDs.

The International Molecular Genetic Study of Autism Consortium [1998] previously identified linkage loci on chromosomes 7 and 2, which were termed AUTS1 and AUTS5, respectively. Further genetic studies have provided evidence for AUTS1 being located on chromosome 7q [The International Molecular Genetic Study of Autism Consortium 2001]. Screening for mutations in six genes mapping to 7q, *CUTL1*, *SRPK2*, *SYPL*, *LAMB1*, *NRCAM*, and *PTPRZ1* in 48 unrelated individuals with autism led to the identification of several new coding variants in the *CUTL1*, *LAMB1*, and *PTPRZ1*genes [Bonora et al., 2005].

The human Ca^{2+}-dependent activator protein for secretion 2 (*CADPS2*: OMIM*609978) is also located on chromosome 7q31, which is within the AUTS1 locus [Cisternas et al., 2003]. It is a member of the CAPS/CADPS protein family that regulates the secretion of dense-core vesicles, which are abundant in the parallel fiber terminals of granule cells in the cerebellum and play important roles in the release of neurotrophin-3 (NT-3) and brain-derived neurotrophic factor (BDNF) [Sadakata et al., 2007a,b,c]. BDNF is indispensable for brain development and function, including the formation of synapses. Cisternas et al. [2003] studied *CADPS2* mutations in 90 unrelated autistic individuals, but identified no disease-specific variants. However, Sadakata et al. [2007a] reported that an aberrant, alternatively spliced *CADPS2* mRNA that lacks exon 3 (*CADPS2* Delta exon3) is detected in some patients with ASD.

Persistent hyperplastic primary vitreous (PHPV) is an ocular malformation caused by the presence of a retrolental fibrovascular membrane and the persistence of the posterior portion of the tunica vasculosa lentis and the hyaloid artery. It is often accompanied by microphthalmos, cataracts, and glaucoma. *NDP* (OMIM *300658, X-linked) and *FZD4* (OMIM *604579, dominant) were found to be mutated in unilateral and bilateral PHPV [Shastry, 2009]. These genes also cause Norrie disease and familial exudative vitreoretinopathy (FEVR), which share some clinical features with PHPV. FEVR is a genetically heterogeneous retinal disorder characterized by abnormal vascularization of the peripheral retina, which is often accompanied by retinal detachment. Mutations in the genes encoding *LRP5* (OMIM *603506, dominant and recessive) also cause FEVR. Junge et al. [2009] showed that *Tetraspanin12* (*Tspan12*) is expressed in the retinal vasculature, and loss of *Tspan12* phenocopies defects are seen in Fzd4, *Lrp5*, and *Norrin* mutant mice. *TSPAN12* is one of the members of the tetraspanin superfamily, characterized by the presence of four transmembrane domains. It constitutes large membrane complexes with other molecules. Nikopoulos et al. [2010] applied next-generation sequencing and found a mutation in *TSPAN12* (MIM*613168). Poulter et al. [2010] described seven mutations that were identified in a cohort of 70 FEVR patients without mutations in three known genes. Mutations in *TSPAN12*, which is at 7q31, are a relatively frequent cause of FEVR.

We performed array comparative genomic hybridization (array-CGH) utilizing a 44K whole genome oligonucleotide microarray in a patient with the ASDs and PHPV. Submicroscopic deletions in 7q31 encompassing *CADPS2* and *TSPAN12* were confirmed. We speculate that haploinsufficiency of *CADPS2* and *TSPAN12* contributes to ASD and PHPV, respectively.

CLINICAL REPORT

The patient, a 3-year-old boy, was born to nonconsanguineous healthy Japanese parents. His family history was unremarkable. He was born at 40 weeks' of gestation, his birth weight was 3,100 g, and his birth length was 50.0 cm. After birth, congenital nystagmus was noted, and he did not pursuit objects. An ophthalmological examination revealed bilateral PHPV. Cataract, glaucoma, and FEVR were not present. His gross motor development was normal, and his verbal development was delayed.

At 3 years of age, he came to our hospital for evaluation because of developmental delay. On examination dysmorphic features included a round face, low-set ears, broad eyebrows, apparent hypertelorism, blepharophimosis, hypoplastic alae nasi, a long philtrum, and a small mouth. His visual acuity was low, but he could perform daily activities with some support. In addition, impairment of social interaction, poor social skills, and strict adherence to routine behaviors were noted. He showed stereotypic movements and hyperactivity in his day care room. He was diagnosed as having an ASD according to the DSM-VI criteria. His DQ was 76 according to standard Japanese method. At 3 years and 8 months of age, his height, weight, and head circumference were 88.6 cm (−2.4 SD), 11.7 kg (−1.8 SD), and 46.8 cm (−2.4 S.D), respectively.

The results of routine laboratory tests were unremarkable. G-banded karyotype analysis revealed the following karyotype: 46,XY,inv(4)(p14;q21). Electroencephalography (EEG) showed occipital epileptic discharges. He was free from epileptic seizures.

Ultrasound evaluation revealed echogenic bands in the posterior segments of both globes. Magnetic resonance brain imaging also showed bilateral fibrous intraocular tissue (Fig. 1). However, no specific findings were found in the CNS including the cerebellum.

FIG. 1. MR coronal image, T2-weighted. Magnetic resonance imaging also showed fibrous intraocular tissue in the eye. [Color figure can be seen in the online version of this article, available at http://onlinelibrary.wiley.com/journal/10.1002/(ISSN)1552-4833]

MATERIALS AND METHODS

After obtaining informed consent based on a permission approved by the institution's ethical committee, peripheral blood samples were obtained from the patient and his parents. Genomic DNA was extracted using the QIAquick DNA extraction kit (QIAgen, Valencia, CA).

Array-CGH analysis was performed using the Human Genome CGH Microarray 44K (Agilent Technologies, Santa Clara, CA), as described previously [Shimojima et al., 2009].

Metaphase nuclei were prepared from peripheral blood lymphocytes using standard methods and were used for FISH analysis with human BAC clones selected from the UCSC genome browser (http://www.genome.ucsc.edu), as described elsewhere [Shimojima et al., 2009]. Physical positions refer to the March 2006 human reference sequence (NCBI Build 36.1).

RESULTS

Using array-CGH analysis, genomic copy number loss was identified in the 7q31.31 region (Fig. 2). The deletion was 5.4 Mb in size and included *CADPS2* and *TSPAN12*, but not *FOXP2*. There were no copy number changes in chromosome 4. FISH analyses confirmed the above deletion (Fig. 3). There were no deletions in either parent indicating de novo occurrence.

DISCUSSION

We described a patient with an ASD and PHPV who demonstrated submicroscopic deletion in chromosome 7q31.31. The deletion resides in the AUTS1 locus on chromosome 7q. The deleted region contained about 20 genes including *CADPS2* and *TSPAN12*. Little data are available about the association of other genes with developmental and ophthalmological disorders. We posit that haploinsufficiency of *CADPS2* and *TSPAN12* contributes to ASDs and PHPV, respectively.

Our patient fulfilled the DSM-VI criteria for an ASD. Poor eye contact, impairment of social interaction, poor social skills with strict adherence to routine, stereotypic movements, and hyperactivity were noted. However, his intellectual disability was mild. Ataxic movement was not observed.

There have been several reports of small deletions on chromosome 7q. Lennon et al. [2007] reported a young male with moderate intellectual disability, dysmorphic features, and language delay who had a deletion in the 7q31.1-7q31.31 region, which included the *FOXP2* gene. The patient demonstrated language impairment, including developmental verbal dyspraxia, but did not meet the criteria for autism. Cukier et al. [2009] reported a chromosomal inversion spanning the region from approximately 7q22.1 to 7q31 in autistic siblings. They suggested that an autism susceptibility gene is located in the chromosome 7q22–31 region. Dauwerse et al.

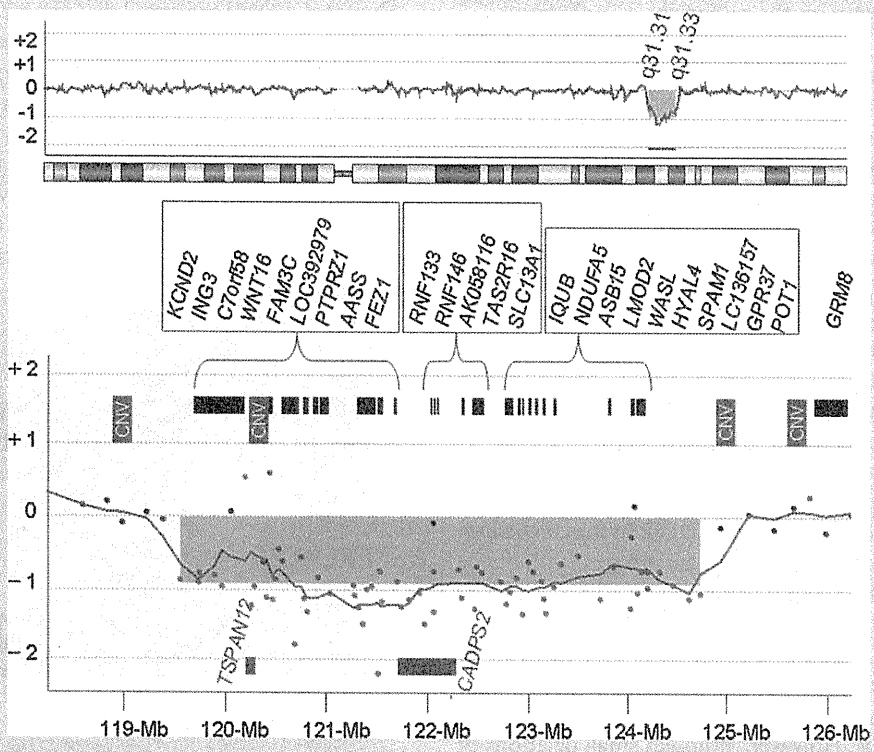

FIG. 2. Array-CGH of the patient. Loss of the genomic copy numbers was identified in the region of 7q31.31. The deletion size was 5.4 Mb and included *CADPS2* and *TSPAN12*.

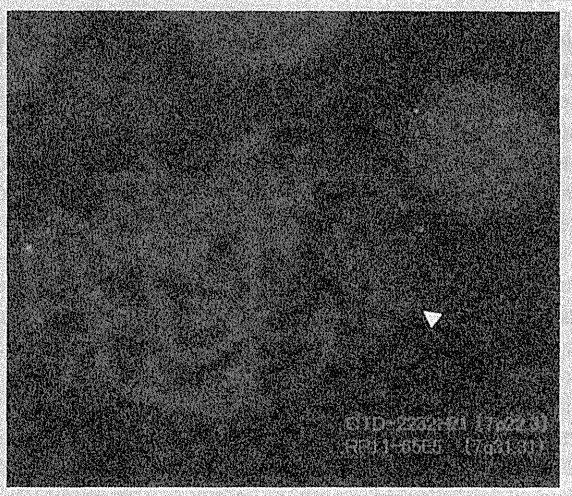

FIG. 3. FISH analyses of the patient. Arrow head indicates the deletion at 7q31.31.

[2010] characterized a de novo complex rearrangement of the long arm of chromosome 7 in a female patient with moderate mental retardation, anxiety disorder, and autistic features and suggested that disruption of the *C7orf58* gene contributed to the anxiety disorder, and autistic features of their patient. The *C7orf58* gene was also deleted in our patient. However, there have been no basic studies on the association of the *C7orf58* gene and brain function. Further studies are necessary on the role of the *C7orf58* gene.

Sadakata et al. [2007b] studied the behavior of *Cadps2−/−* mice. They showed impaired social interaction, hyperactivity, decreased exploratory behavior, and/or increased anxiety in a novel environment and deficits in intrinsic sleep–wake regulation and circadian rhythmicity. In addition, maternal neglect of newborns was a striking feature. They identified that *Cadps2−/−* mice show deficient release of NT-3 and BDNF. Cerebellar development was impaired in the mice. Sadakata et al. [2007a] found an aberrant alternatively spliced *CADPS2* mRNA that lacks exon 3 in some autistic patients. Exon 3 was shown to encode the dynactin 1-binding domain and affect axonal CADPS2 protein distribution. Exon 3-skipped CADPS2 protein possesses almost normal BDNF releasing activity but is not properly transported into the axons of neocortical or cerebellar neurons. However, Eran et al. [2009] observed no difference in prevalence of exon 3 skipping between ASDs and control samples. They concluded that exon 3 skipping represents a normal, minor isoform of CADPS2 in the cerebellum and is likely not a mechanism underlying autism susceptibility or pathogenesis. Our result may reinforce the evidence that *CADPS2* is associated with ASDs.

Cisternas et al. [2003] studied *CADPS2* gene mutations in 90 unrelated autistic individuals. However, they identified no disease-specific variants. Their results indicate that *CADPS2* mutations are not a major cause of ASDs. However, although small deletions of *CADPS2* as found in the present patient, might be rare, they support the idea that *CADPS2* abnormalities are associated with autism susceptibility.

Nikopoulos et al. [2010] reported two missense mutations in five of 11 FEVR families, indicating that mutations in *TSPAN12* are a relatively frequent cause of FEVR. Both residues are completely conserved throughout vertebrate evolution. These authors suggested that both haploinsufficiency and a dominant-negative effect of the mutant TSPAN12 on the wild-type protein should be considered as underlying disease mechanisms. Poulter et al. [2010] described mutations in the *TSPAN12* gene in FEVR patients and suggested that haploinsufficiency of *TSPAN12* causes FEVR because at least four of the seven mutations are predicted to lead to transcripts with premature-termination codons that are likely to be targeted by nonsense-mediated decay.

Recently, the Norrin/Frizzled4 signaling pathway that acts on the on the surface of developing endothelial cells and controls retinal vascular development is highlighted [Ye et al., 2010]. This pathway is composed of Norrin, its transmembrane receptor, Frizzled4, coreceptor, Lrp5, and an auxiliary membrane protein, Tspan12. The resulting signal controls a transcriptional program that regulates endothelial growth and maturation. PHPV and FEVR are associated with their pathogenesis. Our findings indicate that haploinsufficiency of *TSPAN12* is a plausible causative mechanism for PHPV. It will be interesting to study *TSPAN12* abnormalities in PHPV without *NDP* and *FZD4* mutations.

Singh et al. [2006] reported a voltage-gated potassium channel gene mutation in a temporal lobe epilepsy patient, namely a Kv4.2 truncation mutation lacking the last 44 amino acids in the carboxyl terminal. Kv4.2 channel is encoded by the *KCND2* gene. We suggest that the epileptic discharges on EEG reflect neuronal excitability caused by haploinsufficiency of *KCND2*.

Shen et al. [2010] suggested that using chromosomal microarray analysis to test for submicroscopic genomic deletions and duplications should be considered as part of the initial diagnostic evaluation of patients with ASDs. Miller et al. [2010] suggested that the use of chromosomal microarray is recommended as the first-tier cytogenetic diagnostic test for patients with unexplained developmental delay/intellectual disability, ASDs, or multiple congenital anomalies. In patients with ASDs and other anomalies, chromosomal microarray may be the useful method to clarify the underlying defect.

ACKNOWLEDGMENTS

We thank the patient's family for their cooperation. This study was supported by Health and Labour Research Grants from the Ministry of Health, Labour and Welfare of Japan.

REFERENCES

Alarcón M, Abrahams BS, Stone JL, Duvall JA, Perederiy JV, Bomar JM, Sebat J, Wigler M, Martin CL, Ledbetter DH, Nelson SF, Cantor RM, Geschwind DH. 2008. Linkage, association, and gene-expression analyses identify CNTNAP2 as an autism-susceptibility gene. Am J Hum Genet 82:150–159.

Arking DE, Cutler DJ, Brune CW, Teslovich TM, West K, Ikeda M, Rea A, Guy M, Lin S, Cook EH, Chakravarti A. 2008. A common genetic variant in the neurexin superfamily member CNTNAP2 increases familial risk of autism. Am J Hum Genet 82:160–164.